An Euler-Lagrangian coupling method of primary atomization

LIU Chang-bo[1], LEI Fan-pei[2], ZHOU Li-xin[1]

(1. Xi'an Aerospace Propulsion Institute, Xi'an 710100, China;
2. China Aerospace Science and Technology Corporation, Beijing 100037, China)

Abstract: For primary atomization simulations, Direct Numerical Simulation (DNS) requires huge computational resources and time, and simplified models used cursorily in engineering usually give unphysical results. Then a method with hybrid models in different scales is a compromise. An Euler-Lagrangian coupling method of primary atomization is proposed in this paper. The larger liquid blobs are captured by the Volume-of-Fluid (VOF) method, and the droplets comparable with the grid volume or smaller ones are tracked by a two-way coupling LPT model. Since the volume of a Lagrangian Particle Tacking (LPT) particle must be less than 10% of the Lagrangian cell volume, a new LPT method on a virtual mesh is proposed. And a Large Eddy Simulation (LES) model is used to describe the larger vortex structures which are one of the determinants for primary atomization. The developed code is verified by several cases, and some key parameters are investigated to improve its precision. The primary atomization of two impinging jets is calculated by the new method, and the results of instantaneous and time-averaged characteristics show that the new method can give promising prediction.

Keywords: primary atomization; Volume-of-Fluid; Lagrangian particle tracking; large eddy simulation; impinging atomization

CLC Number: V430-34 **Document code**: A **Article ID**: 1672-9374 (2011) 02-0021-12

雾化过程的一种 Euler-Lagrangian 耦合算法

刘昌波[1]，雷凡培[2]，周立新[1]

(1. 西安航天动力研究所，陕西 西安 710100；2. 中国航天科技集团公司，北京 100037)

摘 要：对雾化过程的直接数值模拟需要巨大的计算资源和时间，而工程中的简化模型则经常会给出错误的结果。因此，可以折中地采用一种混合方法，即在不同尺度上采用不同的模型。提出了一种雾化过程的欧拉——拉格朗日耦合算法。较大的液团采用 VOF 法直接求解，与网格尺度相当或更小的液滴则采用双向耦合的拉格朗日粒子法进行追踪。而该方法要求粒子的体积小于网格体积的 10%，为此又提出了一种虚网格粒子追踪法。由于湍流结构对

Received date: 2014-11-26; Revised date: 2015-01-17

Foundation Item: "973" key project of Chinese national programs for fundamental research and development (613193)

Biography: LIU Chang-bo (1979—), male, doctor, speciality: research on liquid rocket engines

雾化过程的影响很大，故湍流采用了大涡模拟模型。采用多个算例对开发的算法进行了验证，并对部分关键参数的影响进行了深入研究。采用新算法对两股撞击射流的雾化过程进行了研究，瞬态和统计结果均表明新算法能够给出良好的预测。

关键词：雾化; VOF 法; 拉格朗日粒子追踪; 大涡模拟; 撞击式

0 Introduction

The atomization is one of the key procedures in liquid-fuel combustors and its characteristics determine the combustion efficiency, combustion stabilization and pollutant emissions. The models often used to simulate the primary atomization are divided into three different levels. Simplified models, such as wave breakup model[1], Taylor analogy breakup model[2] and their deriving/coupling models[3-6], are widely used in engineering. The computational cost is very low, but the accuracy is often doubted. Recently, Direct Numerical Simulations (DNS, often called DNS-like simulations because interface capturing models or turbulent models are also included) are used to investigate primary atomization by many researchers[7-10] with interface capturing models, such as the Volume-of-Fluid (VOF) method, the level set method, etc. However, DNS-like simulations are computationally too expensive, even for solving very simple flow configurations. In fact, the atomization involves motions with temporal and spatial multi scales, and big liquid blobs are larger than the smallest droplets by orders of magnitude. An Euler-Lagrangian Coupling Method (ELCM) adopts hybrid methods at different scales. The larger liquid blobs are modeled by interface capturing approaches to identify the complex process of liquid deformation, breakup and coalescence directly, and major characteristics of the primary atomization are achieved properly. The droplets comparable with the grid volume are simplified to particles to be tracked by a Lagrangian Particle Tracking (LPT) method, so the computational cost decreases rapidly. And an ELCM has advantages of other two methods.

The implementations of an ELCM are quite different. Herrman[11-12] presented an ELCM based on the Refined Level Set Grid Method (RLSGM). At the fully resolved scale, the evolving interface is tracked by RLSGM. When the interface geometry can't be resolved adequately, separated, small scale liquid structures are described by the LPT approach. Grosshans et al.[13] presented an ELCM based on the VOF method. The VOF method was chosen to describe the intact liquid core and dense spray regimes, then the LPT method to describe the dilute spray regime. The statistical parameters of droplet distribution were extracted from the VOF simulation and used to perform Monte-Carlo simulations to create starting conditions for the LPT simulations. Tomar et al.[14] performed an ELCM of primary atomization using a VOF algorithm coupled with a two-way coupling LPT model to simulate the motion and influence of the smallest droplets. The code was implemented in Gerris[15], an open two phase VOF solver. Ma et al.[16] showed good results of two impinging jets using the code. Vallier et al.[17] developed an ELCM to simulate the cavitating hydrofoil, they used the LPT method to track small bobbles generated from liquid. The ELCM is still new and the implementations should be improved further.

A new ELCM for primary atomization is proposed in this paper and implemented in OpenFOAM[18], an open source C++ library. The larger blobs are captured by the VOF approach, and droplets comparable with the grid volume or smaller ones are

tracked by a new two-way coupling LPT model on a virtual mesh. Since the turbulent structures are important to the primary atomization, a LES model is selected. The new algorithm was verified by various test cases. Finally the primary atomization simulation of two impinging jets is presented to demonstrate its excellent performance.

1 Numerical methods

The new ELCM is composed of several methods and modules: the VOF-LES method, the new two-way coupling LPT algorithm on a virtual mesh, identifying droplet module and transforming droplet back module. Also the parallel strategy is very important. The numerical methods are listed in the following subsections.

1.1 VOF-LES method

To describe the simultaneous flow of two immiscible, incompressible fluids, a single set of conservation equations is required for the whole flow field. The mass continuity, momentum and VOF equations are shown as follows:

$$\nabla \cdot \boldsymbol{U}=0 \tag{1}$$

$$\frac{\partial \rho \boldsymbol{U}}{\partial t}+\nabla \cdot(\rho \boldsymbol{U}\boldsymbol{U})=-\nabla p+\nabla \cdot \boldsymbol{\tau}+\rho \boldsymbol{g}+\boldsymbol{S}_P+\int_{S(t)} \sigma \kappa' \boldsymbol{n}' \delta(\mathbf{x}-\mathbf{x}')\mathrm{d}S \tag{2}$$

$$\frac{\partial \alpha}{\partial t}+\nabla \cdot(\alpha \boldsymbol{U})+\nabla \cdot(\alpha(1-\alpha)\boldsymbol{U}_{\mathrm{r}})=0 \tag{3}$$

where $\boldsymbol{U}$ is velocity, ρ is density, p is pressure. The first term on the right hand side of Eq. (2) is the pressure counter gradient, and usually combined with the third term, $\rho \boldsymbol{g}$. The second term is the stress tensor divergence. The forth term, $\boldsymbol{S}_P$, is due to the influence on the flow field of the droplets tracked by the Lagrangian method and will be derived in the next section. The last term represents the source of momentum due to surface tension and acts only at the interface over the entire surface described by $S(t)$, and will be expanded upon later. The liquid volume fraction, α, is introduced for capturing the liquid-gas interface. α may vary from 0 to 1 within a computational cell. Pure liquid is in the cells with α=1 and pure gas with α=0. The interface exists in the cells with intermediate values. The mixture density and viscosity are calculated using:

$$\rho=\alpha \rho_{\mathrm{l}}+(1-\alpha)\rho_{\mathrm{g}} \tag{4}$$

$$\mu=\alpha \mu_{\mathrm{l}}+(1-\alpha)\mu_{\mathrm{g}} \tag{5}$$

where the subscripts l and g are liquid and gas separately. Since the interface is treated as a transitional zone in the VOF method, its exact shape and location are not explicitly known. The surface integral that represents the surface forces cannot be calculated directly. Brackbill et al[19]. overcame this problem with the Continuum Surface Force (CSF) model, which represents the surface tension effects as a continuous volumetric force acting within the transition region. The force is presented in Eq. (6):

$$\int_{S(t)} \sigma \kappa' \boldsymbol{n}' \delta(\mathbf{x}-\mathbf{x}')\mathrm{d}S \approx \sigma \kappa \nabla \alpha \tag{6}$$

where σ is surface tension coefficient, $\boldsymbol{n}$ is unit vector normal to the interface, $\delta(x)$ is Dirac function, $\mathbf{x}$ is the position in the flow field, the curvature of the interface, $\kappa=-\nabla \cdot(\nabla \alpha/|\nabla \alpha|)$, the superscript ' represents the interface.

The necessary compression of the interface is not achieved by using a compressive differencing scheme, but rather by introducing an extra, artificial compression term[20] into Eq. (3). Here, the interface compression equivalent $\boldsymbol{U}_{\mathrm{r}}$ ensures the shrinking of the interface, while the term guaranties both conservation and boundedness[21] of α. The artificial term is only active in the thin interface region. The most general form given by Weller[22] is:

$$\boldsymbol{U}_{\mathrm{r}}=\min(C_\alpha|\boldsymbol{U}|, \max(|\boldsymbol{U}|))\frac{\nabla \alpha}{\nabla \alpha} \tag{7}$$

where the compression velocity $\boldsymbol{U}_{\mathrm{r}}$ is based on the maximum velocity in the interface region. In fact, $\boldsymbol{U}_{\mathrm{r}}$ must be somehow limited, which is achieved using the largest value of the velocity in the domain as the

worst possible case. The intensity of the interface compression is controlled by the constant C_α, which yields no contribution if set to zero, a conservative compression if the value is 1 and an enhanced compression for values greater than 1.

The VOF-LES equations are derived from Eq. (1) ~ Eq. (3) through a localized volume averaging of the phase weighted properties. Filtering removes the very small scales of motion from direct calculation. But several additional terms cannot be directly calculated are produced. For example, the Sub-Grid Scale (SGS) stress, $\tau^{sgs}=\overline{UU}-\overline{U}\ \overline{U}$ (the overlines represent filtering), represents the effect of the unresolved small scales of turbulence. Here it is modeled in eddy viscosity type:

$$\boldsymbol{\tau}^{sgs}-\frac{2}{3}k\boldsymbol{I}=-\frac{\mu^{sgs}}{\rho}\left(\nabla\overline{\boldsymbol{U}}+(\nabla\overline{\boldsymbol{U}})^{T}\right) \tag{8}$$

where the SGS turbulent energy k is calculated from one-equation transport model attributed to Yoshizawa, et al[23]:

$$\frac{\partial k}{\partial t}+\nabla\cdot(k\overline{\boldsymbol{U}})=\nabla\cdot\left[(\nu+\nu^{sgs})\nabla k+\boldsymbol{\tau}^{sgs}\cdot\overline{\boldsymbol{U}}\right]$$
$$-\epsilon-\frac{1}{2}\boldsymbol{\tau}^{sgs}:\left(\nabla\overline{\boldsymbol{U}}+(\nabla\overline{\boldsymbol{U}})^{T}\right) \tag{9}$$

where SGS turbulent dissipation $\epsilon=C_\epsilon k^{3/2}/\Delta$ SGS turbulent kinematic viscosity $\nu^{sgs}=\mu^{sgs}/\rho=C_k k^{1/2}\Delta$, and Δ is the SGS length scale. The constants are $C_\epsilon=1.05$ and $C_k=0.07$.

Additional SGS terms are produced by filtering of the integral in Eq. (2) and the convection term in Eq. (3). The formers are associated respectively to advection, viscous effects, interfacial forces, etc[24]. The latter represents deformation of the liquid-gas interface due to SGS turbulence and will be experienced at the grid scale as an added interphase diffusion. Here all these terms are neglected, following the work of Villiers, et al[25].

1.2 Two-way coupling LPT model on a virtual mesh

A severe error is observed for the convective term in Eq. (2) when the VOF method is used if the diameter of a droplet is less than two-grid length[26]. In this paper the maximum droplet tracked by the LPT method is set to four times of the grid side length. When the diameter of a droplet is less than four times of the grid side length, it may be simplified to a particle. The detailed transformation will be described in the next subsection.

In the Lagrangian frame, a point particle is defined by the position of its center, $\mathbf{x}_P$, its diameter, D_P, its velocity, $\boldsymbol{U}_P$, and its density, ρ_P. If the particle is assumed as s sphere, its volume is $V_P=\pi D_P^3/6$, and its mass is $m_P=\rho_P V_P$. Then the equation of the particle's position and velocity are shown separately as:

$$\frac{\mathrm{d}\mathbf{x}_P}{\mathrm{d}t}=\mathrm{U}_P \tag{10}$$

$$m_P\frac{\mathrm{d}\boldsymbol{U}_P}{\mathrm{d}t}=\sum\boldsymbol{F} \tag{11}$$

where $\boldsymbol{F}$ represents various forces acting on the particle, such as drag force, inertial force, lift force, added mass force, etc. Only the drag force is considered in this paper and the detailed model is same as that described by Vallier, et al[17].

Now the source term $\boldsymbol{S}_P$ in Eq.(2) is discussed. The force exerted by a particle on a unit volume of fluid is proportional to the momentum difference between the instant it enters (t_{in}) and leaves (t_{out}) the control volume cell. Then the additional source term $\boldsymbol{S}_P$ in Eq. (2) is the contribution of this force for each particle which is travelled in the control volume cell:

$$\boldsymbol{S}_P=\frac{-1}{V_i\Delta t}\sum_P m_P\left(\boldsymbol{U}_P(t_{out})-\boldsymbol{U}_P(t_{in})\right) \tag{12}$$

where V_i is the volume of the cell which the particle travels in.

The particles must be much smaller than the Lagrangian grid volume so that they can be approximated as point sources. Even though the results from Arlov et al.[27] show that a particle could

fill up to 22% of the cell volume and still satisfies the LPT theory, the recommended particle volume is usually less than 10% of the Lagrangian grid volume[17]. Because the maximum volume in this study may be larger than the volume of Eulerian cell, the other coarser Lagrangian mesh is needed. But it is not a good idea to use two sets of meshes in a solver. Then a new LPT method of two-way coupling on a virtual mesh is proposed. The Lagrangian mesh is exactly the same as the Euerian mesh, but the particle will affect the current cell and/or its neighbour cells by the source term S_P in Eq.(2). Fig.1 shows the algorithm that a LPT droplet is tracked by the new LPT method on 2D uniform cells.

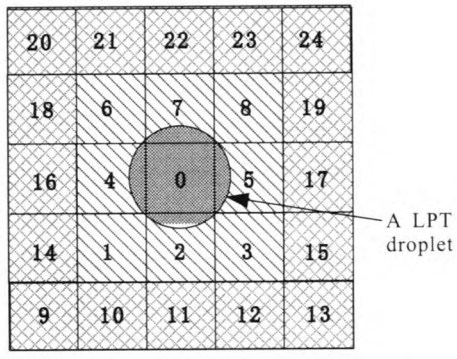

Fig. 1　A LPT droplet affects Eulerian cells (0: Current grid; 1~8: First neighbours; 9~24: Second neighbours.)

It is clear that the LPT droplet is not less than 10% volume of the current cell (0). When tracked by the new method, it will affect the current cell, the first neighbours (1~8) and the second neighbours (9~24) to satisfy the LPT tracking condition. If the side length of a Eulerian cell is l and the volume of the probable biggest droplet is about $4/3\pi\ (2l)^3 \approx 33.5l^3=33.5V_c$, where V_c is the volume of a Eulerian cell. Therefore the maximum volume of the Lagrangian cell must not be less than the sum volume of 335 Eulerian cells. This needs to search the third neighbour cells, and the Lagrangian cell includes $7^3=343$ Euerian cells. Then if only current cell is needed as a Lagrangian cell, S_P only affects the current cell. If the first neighbours are needed, an allocating coefficient β is defined. The source term of the current cell is βS_P and the neighbours' are $(1-\beta)S_PV_i/\sum_{ni}V_{ni}$. If the second neighbours are needed, the current source term is β^2S_P, the neighbours are $(1-\beta^2)S_PV_i/\sum_{ni}V_{ni}$. And so on. The source terms in neighbour cells are proportional to their volume. Thus the two-way coupling LPT method is implemented on a coarser Lagrangian mesh on a finer Eulerian mesh.

1.3　Identifying droplet module

It is very important for an ELCM to identify droplets from the VOF-resolved field. And it's also a very difficult work because the liquid-gas interface is not explicitly described by the VOF method. A connected component technique[15] is selected to identify droplets. The technique is optimized by using a Hash Table (HT) to store all blobs with the key of the cell label and the value of the blob ID. Only the cells containing liquid ($\alpha>0$) are searched to decrease the computational cost. And all their neighbour cells are found out to verify which blob the cell belongs to. If no neighbour cell is found in the HT, this cell must be a new blob, the cell label and the new blob ID are added into the HT. If only one neighbour cell is found in the HT, the two cells must belong to one blob, then the cell is added into the HT with its neighbour blob's ID. If several neighbour cells are found, all these neighbour cells and the current cell should belong to one blob, and all of these cells are connected with their smallest blob ID. All separate blobs are identified out by scanning the α field only once.

The isolated blobs satisfied the following two criterions are transformed to Lagrangian particles. The first criterion is the maximum threshold volume, the other is the droplet sphericity, defined as:

$$\zeta=\frac{R_{\max}}{\max\left[\Delta x,\ (3V_i/4\pi)^{1/3}\right]} \tag{13}$$

where R_{max} is the maximum distance to centre of mass for the blob, Δx is the side length of a cell and V_i is the blob volume. Largely deformed liquid blobs are more probable to experience further break up, which should be captured in the Eulerian representation. The critical value[28] is typical ζ=4. If the blob is transformed to a Lagrangian point particle, extra process should be done. The liquid fraction α of associated cells are set to zero. The location, mass and average momentum of the blob are assigned to the representative particle.

1.4 Transforming droplet back module

If a LPT particle impacts the VOF resolved large blob, the particle must be transformed back to continuous field. Otherwise it is unphysical to track a LPT droplet in the VOF resolved blobs. Since the exact interface is unknown for the VOF method, it is difficult to determine the exact instant to impact. Here a lower limit α_{lim1} is defined. When the volume fraction of the cell which a LPT droplet travels in reaches to α_{lim1}, the droplet is transformed back to the continuum field. If a particle is determined to be transformed back, the LPT droplet is removed from the storing table, then its mass and momentum are transformed back to the VOF resolved fields. If the current cell is overflow, the extra part of the particle will be distributed into the vacuum neighbor cells.

1.5 Parallel processing strategy

The method of parallel computing used by OpenFOAM is known as domain decomposition, in which the geometry and associated fields are broken into pieces and allocated to separate processors for solution. If a cell is adjacent to a processor patch, its neighbour cell s may be located in neighbour processors. The standard solver can't find the neighbour cells in other processors. Therefore a proper strategy must be taken to access neighbour cells in neighbour processors.

A preprocessing module is build to find out all neighbour cells in neighbour processors. Firstly the points in processor patches are found out and their connected cells in current processor are searched out too. Secondly these points and their connected cells are sent to neighbour processors. Then the corresponding points (exactly the same point in serial computation) are found out based on these point coordinates. Thus the neighbour cells in neighbour processors can be determined. Finally the properties of cells in neighbour processors including the volume, liquid fraction, velocity, etc. are transferred to corresponding processors. All of neighbour cells in current and neighbour processors are found out entirely. This parallel processing will occupy a little longer time at the beginning of the code. And when the iteration starts, the update time of each step is very short.

The new ELCM based on a VOF method is implemented successfully in the OpenFOAM platform. A LES model with single k equation is selected for turbulent simulation. A two-way coupling LPT method on a virtual mesh, the identifying droplet module, the transforming droplet back module, etc. are built in the new algorithm. Next section will emphsize on the verifications of these new models and modules.

2 Numerical verifications

2.1 Identifyingadropletfrom VOF-resolvedfields

A case without turbulent models is designed to verify the identifying ability. The fluid parameters are shown in Tab.1. A lower limit α_{lim0} is defined here, and only the cells with liquid volume fraction above α_{lim0} are scanned in the blob's identification. A VOF resolved droplet is initialized in the continuum fields, the identifying results according to different α_{lim0} are presented in Fig.2. The diameter and momentum of the LPT droplet are both becoming smaller with larger α_{lim0}. When α_{lim0} is larger, the cells with less liquid in the droplet are abandoned. For example, there is a VOF resolved droplet in Fig.3, if α_{lim0}=0.001 and all of the nine cells are identified; if

α_{lim0}=0.01 and eight cells are identified out; if α_{lim0}=0.1 and only seven cells are identified out. Thus the volume of the identified droplet is smaller with larger α_{lim0} and that is true for the diameter changing. The momentum is smaller with more cells abandoned. But if α_{lim0} is set too small, numerical problems may misconnect some neighbour droplets or some virtual droplets will be appeared. A compromise value is chosen as α_{lim0}=0.01 based on many numerical experiments.

Tab.1　Characteristics of the fluids

Liquids	Density /(kg·m^{-3})	Viscosity /(m^2·s^{-1})	Surface tension /(kg·s^{-2})
Air	1.205	1.5×10^{-5}	–
Water	998.2	1.003×10^{-6}	0.072 8

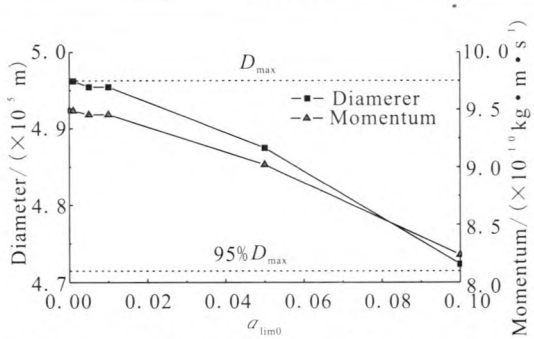

Fig. 2　Diameter/momentum of identifying results vs α_{lim0}

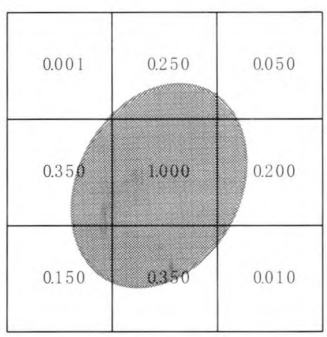

Fig. 3　A droplet in VOF resolved field

2.2　Two-way coupling LPT method on a virtual mesh

The geometry setup of a verification case is shown in Fig.4 and the main parameters of the fluids are shown in Tab.1. Each side of the cube is 1.0 mm, the lower half is filled with water and the upper is air. A droplet is initialized at 0.2 mm above the water surface, and it's diameter is about 50 μm. It's initial velocity is -15 m/s along z axis. A sampling line is set in the middle of the droplet's initial position and the water surface. The sampling time is 10 μs when the droplet has just passed the sampling line. The domain is decomposed into 50×50×50 cells. The momentum allocating coefficient β is an important parameter for the two-way coupling LPT method on a virtual mesh. β affects the momentum distribution among the current cell and its neighbours. Then the velocity on the sampling line is selected to compare the influences of β.

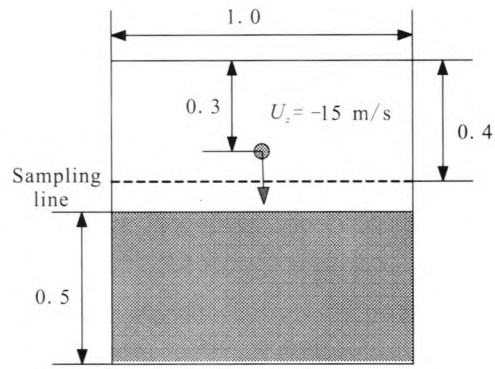

Fig. 4　A droplet falls into water (Unit: mm)

Because the absolute velocity differences are too small to compare the β influences, the relative velocity to β=0.1 is selected to investigate the influences of β, shown in Fig.5. The velocity near the droplet is higher as β becomes larger. When β is larger, the LPT droplet affects more on current cell, and the velocity changes of the current is larger too. If β=1.0, the LPT droplet only affects the current cell, but it isn't on a virtual mesh yet. Furthermore there is a serious disturbance on the current cell by large LPT droplets and it isn't good for the calculating convergence. On the other hand, too small value of β is not advised because it's not obvious to distinguish the more influence on the located cell than on its neighbours. For a uniform 3D mesh, if only the first neighbours are needed, the

lowest limit of β is 1/27 ≈0.037, when the momentum allocates to the current and its neighbours equally. The compromise value of β is selected as 0.2 based on many numerical tests.

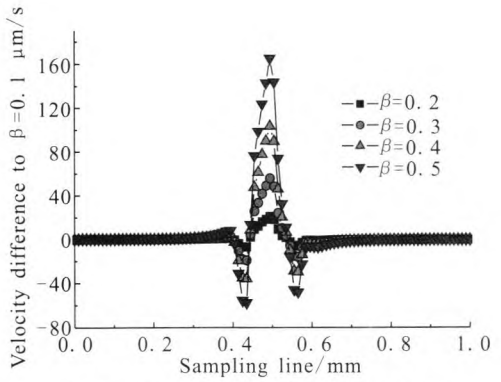

Fig. 5 ΔU based on β=0.1 at 10 μs

2.3 A LPT droplet transforms back

When a LPT droplet impacts a large VOF resolved blob, it will be transformed back to the VOF resolved fields including the mass and momentum. It is also hard to determine the lower limit α_{liml} since the exact liquid-gas interface is not explicitly calculated by the VOF method. If α_{liml} is set too small, the impact probability will be higher than the truth because some LPT droplets may not really impact into the large blobs. While α_{liml} is set too large, some LPT droplets may move in the VOF blobs. Therefore, a compromise value of 0.5 is chosen finally.

The configuration of the case is the same shown in Fig.4, but pure VOF method is also used to compare the results. After the droplet impacted the water surface at 13.5 μs, Fig.6 shows the results of the two methods at 20 μs. The droplet has disappeared when it is impacted the water surface. The detailed results show that the mass and momentum of the LPT droplet are transformed successfully back to the continuum fields, and the impacted positions are clearly concave. The velocity vector is similar for the two methods, and the velocity near the droplet trajectories is higher and two recirculations have appeared on both sides of the trajectories. However it is obvious that the fluid velocity of the VOF method is stronger and the concaveness is larger. The results show that the coupling intensity between the LPT droplet and the continuum fields is a little weaker for the ELCM. Also the reaction of the surface is slower. Anyway the ELCM can simulate the impacting process properly.

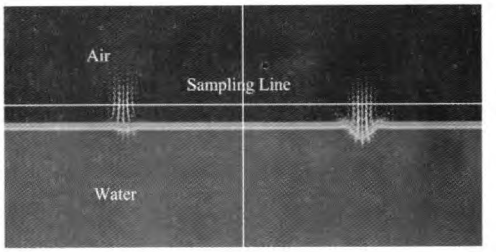

(a) ELCM (b) Pure VOF method

Fig. 6 A droplet impacted the water surface

2.4 Parallel computing tests

It is important to build a parallel code to simulate complex cases by multiple processors. A simple case with 18 droplets is set to verify the parallel strategy of the ELCM and six of them are crossing two CPUs. After several iterate steps, the droplets across two CPUs are identified successfully and tracked correctly by the new LPT method on a virtual mesh. The results show that the parallel processing strategy implements well.

The verification results show that each part of the new ELCM can run correctly. Next a more complex case is used to verify the new method comprehensively.

3 Primary atomization simulation of like-doublet jets

Verification results of several simple cases show that each part of the new ELCM code works well. Then the primary atomization of two impinging jets is simulated by the new ELCM. And the simulation results will be compared with the experimental data.

3.1 Problem description

Fig.7 shows the computational domain and boundary conditions. Two water jets at 90° are injected into a box of $40d\times12d\times20d$ (x, y, z in turn), where d is the diameter of the two inlet orifices. The box size includes the breakup length of the formation sheet from experimental results [29]. The diameter d=1.0 mm. The magnitudes of inlet average velocity are 30 m/s. The fluid characteristics are shown in Tab.1. And Re and We of a jet are about 3×10^4 and 1.2×10^4 respectively. A coordinate is shown in Fig.8 for description convenience. The geometry and mesh are generated by ICEM software of ANSYS. The grids should be small enough near the wall for the LES simulation. However the computer at hand is not powerful and the number of cells is only about 3.0 million. At this time, dimensionless wall distance y^+ of the first grid height near the wall is about 5. The total calculating time is more than one month on 32 cores of the Xeon 2.8 GHz.

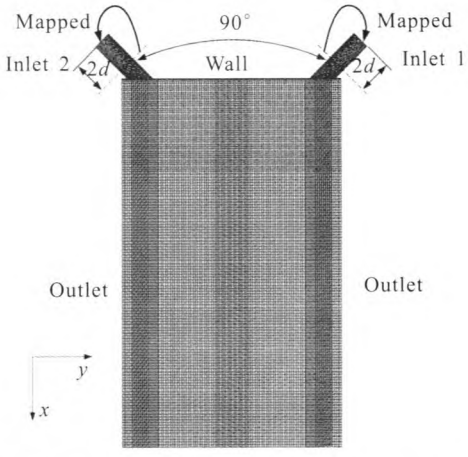

Fig. 7 Computational grids and boundary conditions

Each jet is set to a fully developed turbulent flow similar to reference [25]. Then a "Mapped" cond- ition is applied to each inlet and the mapped plane is $2d$ downstream the inlet. The column surfaces of the inlets and the upper side of the box are set to no slip "Wall" conditions, other sides are the "Outlet" conditions.

The initial conditions are a little difficult to imple-ment. Firstly fully developed turbulent flow in two pipes should be calculated for the two inlets. Many researchers investigated the pipe turbulent flow by DNS or LES. Eggels et al.[30] considered it was enough to select the pipe length of $5d$, but $2\pi d$ is used here just as Rudman et al. [31]did. The "cyclic" conditions are adopted in the pipe streamwise. The pipe flow is initialized by using a laminar parabolic profile and near-wall parallel streaks of slower and faster moving fluid are produced by modifying this base parabolic flow. Then the flow produces streamwise vortices by slight perturbations after some time. The fully-developed turbulent flow is achieved after about 20 flow-through times [32]. Secondly the fully-developed turbulent flow in a pipe is allocated to two inlet orifices. The calculation time is set to more than two flow-through times based on bulk inlet velocity, it's about 2 ms. The time-averaged properties are extracted from the ELCM simulations.

The instantaneous features and the time-averaged properties are listed in the following.

3.2 Instantaneous spray morphology

Fig.8 shows the instantaneous spray morphology coloured by the local velocity magnitude. The two fully-developed turbulent jets impact to form a liquid sheet, the sheet waves to breakup into fragments and ligaments after several wave length. The charac-teristics of the wave breakup are considered to relate to the combustion instability[10]. Then the fragments and ligaments breakup into larger blobs and finer droplets. The jets, sheet, ligaments and larger blobs are captured by the VOF method, and the finer droplets are tracked by the LPT method on a virtual mesh. It's similar to the experimental results of a laser holograph and image processing method in Fig. 9. The breakup length[33] of the liquid sheet is defined as the distance from the impingement point to the edge of liquid sheet along x axis as shown in Fig.7.

The breakup length is about 11 mm close to the experimental value of 11.8 mm.

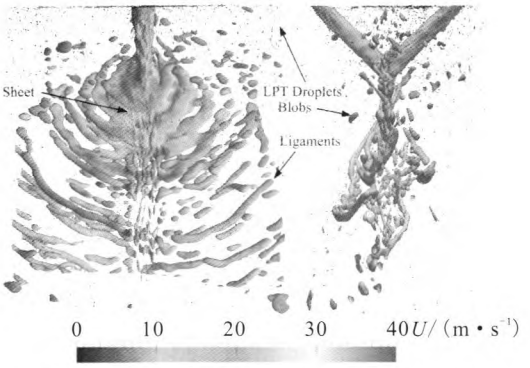

Fig. 8 α=0.1 isosurface of front/side view

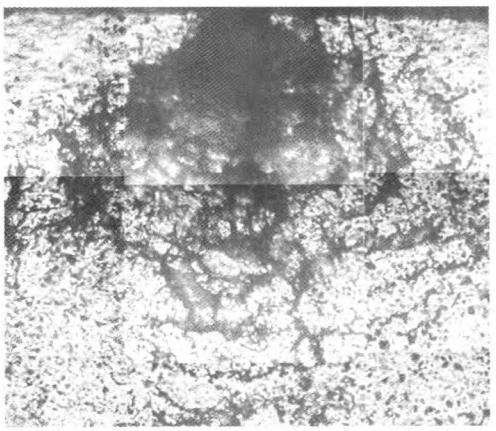

Fig. 9 Front view of experimental results

3.3 Time-averaged properties

The spray angle is extracted from the simulation results by the following approach. The isosurface of α=0.1 is drawn for each time step, and the spreading edges around the impact point in the front view can be clearly distinguished. The angle between the two lines along the spreading edge can be measured. The final value of the spray angle is averaged out by these instantaneous angles. The simulated value is about 105° and good agreement with the experimental value of about 110° .

The probability density distribution of the droplet diameter is shown in Fig.10. The smaller droplets are deleted from the statistics because the experiment apparatus can only identify the droplets larger than 15 μm. The biggest diameter is set to 300 μm according to the experiment results. The sampling region is selected similar to the processing of the experiment data. It is set to the last 10 mm domain along x axis. The curve from simulation results is agreed well with that of the experimental results.

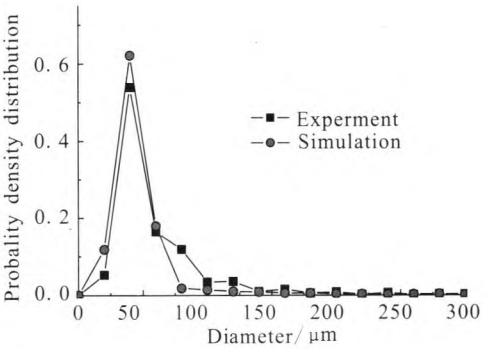

Fig. 10 Probability density distribution of the droplet diameter

The instantaneous and time-averaged results show that the ELCM can give a prospective prediction for the complex atomization of the impinging jets.

4 Conclusions

A new ELCM is proposed for primary atomization in this paper. The large blobs are captured by the VOF algorithm and their detailed changes are more accurate than those simplified models. The small droplets are tracked by a new LPT model on a virtual mesh and the computational cost is much less than the DNS-like simulations. The turbulent flow is simulated by a LES model. Also some additional modules and functions are developed to implement an integrated code.

The new code is verified for every new module, and the results show that all parts work well. The primary atomization of the impinging jets is simulated by the new code, and the results are good agreement with the experimental results. This indicates that the

new ELCM can apply prospectively to the complex primary atomization in engineering.

References:

[1] REITZ R D. Modeling atomization processes in high-pressure vaporizing sprays[J]. Atomization and Spray Technology, 1987, 3(4): 309-337.

[2] O'ROURKE P J, AMSDEN A A. The TAB method for numerical calculation of spray droplet breakup [R]. USA: SAE, 1987.

[3] HUH K Y, GOSMAN A D. A phenomenological model of diesel spray atomization[C]// Proceedings of International Conference for Multiphase Flow. Japan: University of Tsukuba, 1991: 24-27.

[4] CHANG S K, KOO J Y, CHUNG H C. Transient liquid jet breakup model and comparison with phase Doppler measurements[J]. KSME International Journal, 1995, 9(1): 41-50.

[5] KOO J Y. An overview of liquid spray modeling formed by high-shear nozzle/swirler assembly[J]. KSME International Journal, 2003, 17(5): 726-739.

[6] TRINH H P, CHEN C P. Modeling of turbulent effects on liquid jet atomization and breakup, AIAA-2005-154 [R]. USA: AIAA, 2005.

[7] DESJARDINS O, MOUREAU V, PITSCH H. An accurate conservative level set/ghost fluid method for simulating turbulent atomization [J]. Journal of Computational Physics, 2008, 227(18): 8395-8416.

[8] FUSTER D, BAGUE A, BOECK T, et al. Simulation of primary atomization with an octree adaptive mesh refinement and VOF method[J]. International Journal of Multiphase Flow, 2009, 35(6): 550-565.

[9] IANG X, SIAMAS G A, JAGUS K, et al. Physical modelling and advanced simulations of gas-liquid two-phase jet flows in atomization and sprays[J]. Progress in Energy and Combustion Science, 2010, 36(2): 131-167.

[10] CHEN X D, MA D J, YANG V. Mechanism study of impact wave in impinging jets atomization, AIAA-2012-1089[R]. USA: AIAA, 2012.

[11] HERRMANN M. Refined level set grid method for tracking interface [R]. USA: Center for Turbulence Research, Stanford University, 2005.

[12] HERRMANN M. A parallel Eulerian interface tracking/Lagrangian point particle multiscale coupling procedure [J]. Journal of Computational Physics, 2010, 229 (3): 745-759.

[13] GROSSHANS H, SZ?SZ R Z, FUCHS L. Full spray simulation-coupled volume of fluid and Lagrangian particle tracking methods[C]// 24th European Confer-ence on Liquid Atomization and Spray Systems. Estoril, Portugal:[s.n.],2011: 120-128.

[14] TOMAR G, FUSTER D, ZALESKI S, et al. Multiscale simulations of primary atomization[J]. Computers & Fluids, 2010, 36(10): 1864-1874.

[15] POPINET S. Gerris: a tree-based adaptive solver for the incompressible Euler equations in complex geometries [J]. Journal of Computational Physics, 2003, 190 (2): 572-600.

[16] MA D, CHEN X, KHARE P, et al. Atomization pat-terns and breakup characteristics of liquid sheets formed by two impinging jets, AIAA-2011-97[R]. USA: AIAA, 2011.

[17] VALLIER A, REVSTEDT J, NILSSON H. Procedure for the break-up of cavitation sheet[C]// 4th Interna-tional Meeting on Cavitation and Dynamic Problems in Hydraulic Machinery and Systems. Belgrade, Serbia, 2011: 111-120.

[18] WELLER H G, TABOR G, JASAK H, et al. A tensorial approach to computational continuum mechanics using object-orientated techniques[J]. Computers in Physics, 1998, 12(6): 620-630.

[19] BRACKBILL J U, KOTHE D B, ZEMACH C. A continuum method for modeling surface tension[J]. Journal of Computational Physics, 1992, 100(2): 335-354.

[20] RUSCHE H. Computational fluid dynamics of dispersed two-phase flows at high phase fractions[D]. London: Diploma of Imperial College, University of London, 2002.

[21] BERBEROVICE. Investigation of free-surface flow associated with drop impact: numerical simulations and theoretical modeling [D]. Germany: Bosnien und Herzegowina, Technischen Universität Darmstadt zur, aus Zenica, 2010.

[22] WELLER H G. A new approach to VOF-based interface capturing methods for incompressible and compressible flow [R]. [S.L.]:OpenCFD Ltd., 2008.

[23] YOSHIZAWA A, HORIUTI K. A statistically-derived subgrid-scale kinetic energy model for the large-eddy simulation of turbulent flows[J]. Journal of the Physical Society of Japan, 1985, 54(8): 2834-2839.

[24] TOUTANT A, LABOURASSE E, LEBAIGUE O, et al. DNS of the interaction between a deformable buoyant

bubble and a spatially decaying turbulence: A priori tests for LES two-phase flow modeling[J]. Computers and Fluids, 2008, 37(7): 877-886.

[25] VILLIERS E D, GOSMAN A D, WELLER H G. Large eddy simulation of primary diesel spray atomization, 2004-01-0100 [R]. USA: SAE, 2004.

[26] ERNE G, PETELIN S, TISELJ I. Numerical errors of the volume-of-fluid interface tracking algorithm[J]. International Journal for Numerical Methods in Fluids, 2002, 38 (4): 329-350.

[27] ARLOV D, REVSTEDT J, FUCHS L. A different approach for handling large bubbles in a square cross-sectioned bubble column combining large eddy simulation with Lagrangian particle tracking[C]// 6th International Conference on Multiphase Flow. Leipzig, Germany: [s. n.], 2007: 56-62.

[28] LI X Y, SOTERIOU M C. Prediction of high density-ratio liquid jet atomization in crossflow using high fidelity simulations on HPC, AIAA-2012-0175[R]. USA: AIAA, 2012.

[29] ZHANG M, ZHANG Z, LI A, et al. Experimental research on spray properties of unlike impinging injectors [J]. Journal of Propulsion Technology, 2000, 21 (1): 57-59. (in Chinese)

[30] EGGELS J, UNGER F, WEISS M, et al. Fully developed turbulent pipe flow: a comparison between direct numerical simulation and experiment[J]. Journal of Fluid Mechanics, 1994, 268(12): 175-209.

[31] RUDMAN M AND BLACKBURN H M. Large eddy simulation of turbulent pipe flow[C]// Proceedings of Second International Conference on CFD in the Minerals and Process Industries, Melbourne, Australia: CSIRO, 1999: 23-30.

[32] VILLIERS E D. The potential of large eddy simulation for the modeling of wall bounded flows[D]. London: Imperial College of Science, 2006.

[33] JUNG K, KHIL T, YOON Y, et al. The breakup characteristics of liquid sheets formed by like-doublet injectors, AIAA-2002-4177[R]. USA: AIAA, 2002.

(编辑：马 杰)

(上接第 12 页)

[2] ZHANG T P. Initial flight test results of the LIPS-200 electric propulsion system on SJ-9A satellite, IEPC-2013-47[R]. USA: IEPC, 2013.

[3] ZHANG T P. The LIPS-200 ion electric propulsion system development for DFH-3B satellite platform, IAC13-C4. 4.10[R]. China: [s.n.], 2013.

[4] 张天平. LIPS-200 离子推力器寿命地面试验方案研究[J]. 航天器工程, 2012, 21(4): 111-116.

[5] ZHANG T P. Electric propulsion development for DFH-4SP satellite platform, IAC-14-C4.4.2[R]. Isreal: [s.n.], 2014.

[6] HANI K. Operational status of the international space station plasma contactor hollow cathode assemblies, AIAA 2011-5990[R]. USA: AIAA, 2011.

[7] CORBETT M H .Thrust control algorithms for the GOCE ion propulsion assembly, IEPC-2007-210 [R]. USA: IEPC, 2007.

(编辑：陈红霞)